Available online at www.sciencedirect.com
SCIENCE DIRECT®
Journal of Nuclear Materials 337–339 (2005) 291–295
journal of nuclear materials
www.elsevier.com/locate/jnucmat

Generation of toroidal rotation by gas puff. Simulations of MAST experiments with B2SOLPS5.0

V. Rozhansky [a,*], E. Kaveeva [a], S. Voskoboynikov [a], G. Counsell [b], A. Kirk [b], D. Coster [c], R. Schneider [d]

[a] St. Petersburg State Polytechnical University, Polytechnicheskaya 29, St. Petersburg 195251, Russian Federation
[b] EURATOM/UKAEA Fusion Association, Culham Science Centre, Abingdon, Oxon, OX14 3DB, UK
[c] Max-Planck Institut für Plasmaphysik, EURATOM Association, D-85748 Garching, Germany
[d] Max-Planck Institut für Plasmaphysik, EURATOM Association, D-17491 Greifswald, Germany

Abstract

Simulations have been performed to investigate the impact of gas puffing position on plasma toroidal rotation. It was demonstrated that inboard puffing generates counter-current rotation in agreement with experimental observations. On the basis of the simulations a physical model was put forward, which is based on momentum transport by vertical ∇B drifts and anomalous radial transport. Toroidal rotation is generated mainly due to radial transport of the inboard/outboard particle fluxes by ∇B drifts. Its value depends on the location, radial and poloidal dimensions of the ionization source on the closed field lines, increases linearly with the ion temperature and plasma density and is inversely proportional to the plasma current.

PACS: 52.25.Fi; 52.55.Fa; 52.65.−y
Keywords: Edge modelling; MAST

1. Introduction

In recent experiments on MAST [1] it was observed that toroidal rotation inside the separatrix depends on the position of the gas puff. For the inboard puff the rotation at the low field side (LFS) was counter-current directed while for outboard puff the direction of toroidal velocity was co-current. Moreover, the inboard gas puff reduced the L–H transition threshold. Co-current toroidal rotation at the outer midplane for ion ∇B drift directed towards the X-point has been observed in the SOL on several tokamaks [2–4]. The simulations with B2SOLPS5.0 [5], UEDGE [6] and EDGE2D [7] reproduced rotation in the same direction.

In the present paper a comparative simulation of two similar MAST L-mode shots has been performed with the code B2SOLPS5.0, for two position of gas puff. The observed change of toroidal rotation has the same tendency as in the experiment. The inboard gas puff creates a high field side (HFS) source of ionization on the closed flux surfaces. As a result the inboard–outboard parallel fluxes arise. The transport of these fluxes by the vertical ion ∇B drifts produces a torque in the counter-current direction. This torque results in the change of

* Corresponding author. Tel./fax: +1 812 5527954.
E-mail address: rozhansky@phtf.stu.neva.ru (V. Rozhansky).

0022-3115/$ - see front matter © 2004 Elsevier B.V. All rights reserved.
doi:10.1016/j.jnucmat.2004.10.080

average toroidal rotation, which is damped by anomalous viscosity.

2. Simulation results

Two L-mode Disconnected Double Null MAST discharges nos. 6467 and 6468 with similar geometry (active lower divertor) were chosen. The following modelling parameters were taken: anomalous diffusion coefficient $D = 1.5\,m^2/s$, electron and ion heat conductivity $\kappa_e/n_e = 2.5\,m^2/s$, $\kappa_i/n_e = 3.75\,m^2/s$. The plasma density at the inner boundary of calculational domain (6 cm inside the separatrix at the outer midplane) was $n_e|_{core} = 1.75 \times 10^{19}\,m^{-3}$, the electron and ion temperatures are $T_e|_{core} = 120\,eV$, $T_i|_{core} = 120\,eV$. Initially gas puff of $\Gamma = 6.3 \times 10^{21}\,s^{-1}$ was imposed at the outer midplane for shot no. 6467 and $\Gamma = 2.1 \times 10^{21}\,s^{-1}$ at the inner midplane for the shot no. 6468. The simulation with inboard gas puff $\Gamma = 6.3 \times 10^{21}\,s^{-1}$ was also performed. In spite of the fact that in the experiment the HFS gas puff was three times smaller, this simulation case could be rather representative, see discussion below. The experimentally observed electron temperature and density radial profiles at the outer and inner midplanes as well as the saturation current and electron temperature distributions at the divertor plates are reproduced in the simulations with reasonable accuracy. The calculated and measured toroidal velocities in the core, Fig. 1, are of the same order and change similarly while switching from the outer to the inner midplane gas puffing (the increase of calculated core velocity is 2.7 km/s for large inboard gas puffing and 0.9 km/s for small puffing). In the SOL, where the accuracy of measurements is worse, the calculated toroidal velocity is larger than in the experiment. The poloidal profiles of the parallel velocity in the core are shown in Fig. 2(a)–(c). For the LFS gas puff, Fig. 2(c), the parallel velocity is of the Pfirsch–Schlueter (PS) type while for the HFS, high gas puffing

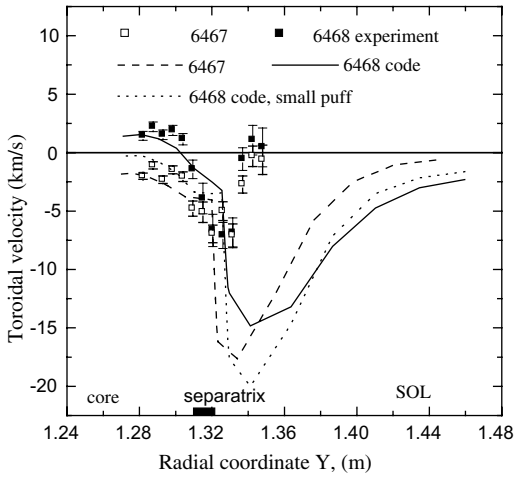

Fig. 1. Toroidal velocity at the outer midplane for shots no. 6467 (outboard puff) and no. 6468 (inboard puff). Simulation result with large HFS puff is also shown.

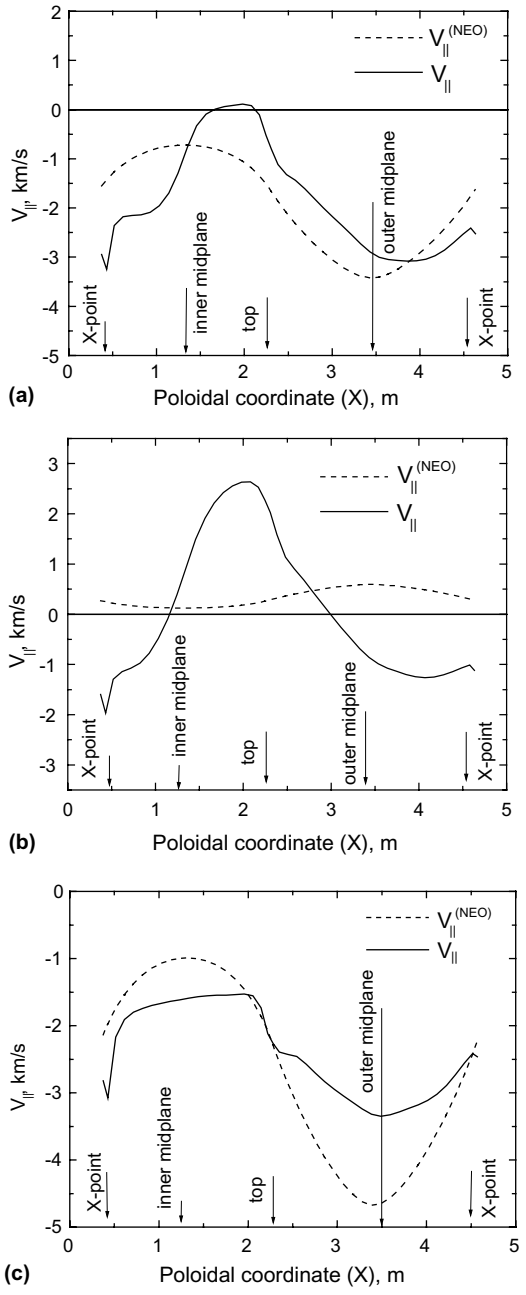

Fig. 2. Poloidal profile of parallel velocity in the core (15 mm from the inner separatrix at the outer midplane). (a) shot no. 6468, small inboard puff, (b) shot no. 6468, large inboard puff, and (c) shot no. 6467, outboard puff.

case, Fig. 2(b), the pattern is completely different from that of the PS type. The pronounced fluxes from the inboard to the outboard midplane are clearly seen. Since the additional parallel fluxes are proportional to the ionization source, for low gas puffing, Fig. 2(a), these fluxes are less pronounced.

The mechanism responsible for the toroidal torque is illustrated schematically in Fig. 3. In the upper part of the torus the vertical ∇B drift transports positive (counter-current) momentum inwards creating positive torque. In the lower part the negative parallel momentum is transported downwards again producing positive torque. This torque is balanced mainly by the radial transport of toroidal momentum due to anomalous viscosity and diffusion, Fig. 4(a) and (b). For inboard gas puffing, Fig. 4(a), the radial flux of toroidal momentum associated with ∇B drift and the flux caused by the anomalous viscosity and diffusion, which compensates it, are the largest contributions to the momentum balance. For outboard gas puffing, Fig. 4(b), these fluxes are smaller. One can see that the mechanism proposed in [8] does not play a significant role since anomalous transport of toroidal momentum dominates over neutral viscosity (curves 1 and 3). Note that this remains true for the wide range of possible anomalous transport coefficients. The effect considered is also significantly larger than the

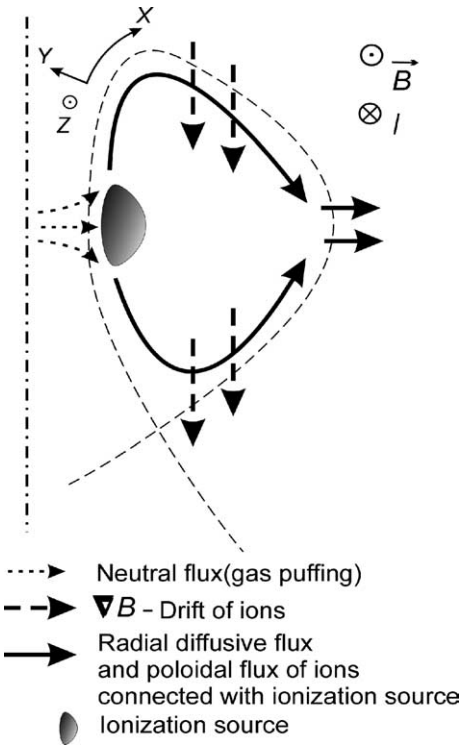

Fig. 3. Schematic of the particle fluxes in the discharge with inboard puff.

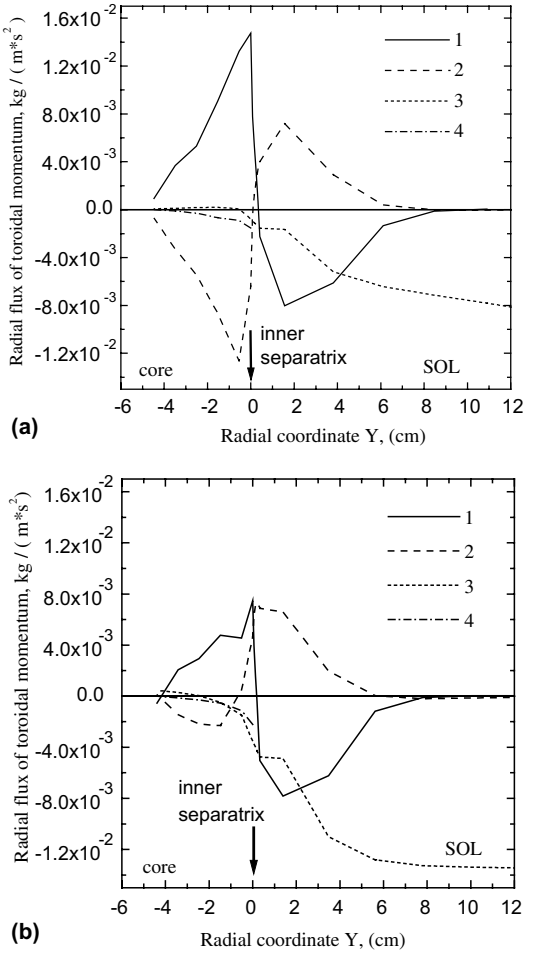

Fig. 4. Components of the average flux of parallel momentum through the flux surface. (1) flux associated with anomalous viscosity and diffusion; (2) flux associated with ∇B. drift; (3) radial flux of toroidal momentum for neutrals; and (4) change of the radial flux of toroidal momentum due to neoclassical torque calculated according to [9]. (a) shot no. 6468 large inboard puff, and (b) shot no. 6467, outboard puff.

change of the mometum flux due to existence of the neoclassical torque [9].

In the real experiment the inboard puff was about three times smaller than that for outboard case and was strongly toroidally localized. The effect on toroidal rotation in the corresponding simulation is modest. For larger HFS gas puff the change of rotation is more pronounced. It is in the same direction and all other effects are also similar. In the simulations with large HFS gas puff, in addition to the ionization source on the closed flux surfaces created by direct penetration of neutrals an effective source was also produced by an inward diffusive ion flux caused by the inversion of the ion density profile near the gas injector. For smaller HFS

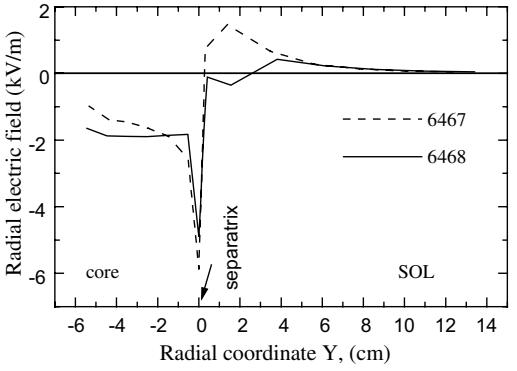

Fig. 5. Radial electric field at the outer midplane for shots no. 6467 (outboard puff) and no. 6468 (large inboard puff).

injection no inversion of the density profile is observed and the whole effect is weaker.

In the simulation a toroidally uniform inboard injection has been imposed, while in the real experiment the injection took place at a specific toroidal position. It is possible that in the real experiment the inversion of the density profile exists in the vicinity of the injector, which might amplify the whole effect. It is also possible that for the toroidally non-uniform injection neutral penetration is deeper, which also results in a larger change of the toroidal rotation in the core. In the future experiments on MAST toroidally uniform gas puff is planned so the effect will be tested.

The radial electric field for the two shots is shown in Fig. 5 for the case of equal LFS/HFS gas puff. In the case of HFS puff the radial electric field in the core is more negative in accordance with its neoclassical character and the change in toroidal rotation velocity. However, in the core the shear of electric field is even smaller for HFS gas puff. In general it is difficult to judge on the shear of electric field, which is the key issue for the L–H transition.

3. Analytical estimates

Consider the radial flux of toroidal momentum. The condition of zero average current through the flux surface can be expressed from toroidal momentum balance [10] ($\langle\langle F\rangle\rangle \equiv \oint F h_x h_z \,\mathrm{d}x / \oint h_x h_z \,\mathrm{d}x$, x and y are coordinates along and across the flux surfaces accordingly, z is the toroidal direction, $\vec{b} = \vec{B}/B$):

$$\frac{1}{h_y h_z B_x}\frac{\partial}{\partial y}\left\langle\left\langle h_z\left(m_i n V_y V_z - \eta\frac{\partial V_z}{h_y \partial y}\right)\right\rangle\right\rangle = \left\langle\left\langle\frac{F_z}{B_x}\right\rangle\right\rangle, \tag{1}$$

where $h_x = \frac{1}{\|\nabla x\|}$, $h_y = \frac{1}{\|\nabla y\|}$, $h_z = \frac{1}{\|\nabla z\|}$, $\sqrt{g} = h_x h_y h_z$, F_z is an ion-neutral friction force. The calculations demonstrate that the r.h.s. of Eq. (1) may be neglected. Without puff the average toroidal velocity is determined by the balance between the momentum flux connected with anomalous viscosity (second term on the l.h.s.) and the momentum flux corresponding to the diffusive flux of particles (first term on the l.h.s.). With the gas puff an additional convective toroidal momentum torque arises, Fig. 3.

The parallel velocity associated with the location of the particle source can be found using the model particle continuity equation

$$\frac{1}{\sqrt{g}}\frac{\partial}{\partial x}\left[\frac{\sqrt{g}}{h_x} n b_x V_\parallel\right] = I(x,y) - n/\tau(x,y). \tag{2}$$

Here I is the particle source while τ represents the diffusive escape of particles. The parallel velocity created by the source together with the average parallel velocity is:

$$V_\parallel = \frac{B}{n}\int_{\mathrm{in}}^{x}[I(x',y) - n/\tau(x',y)]\frac{h_x \mathrm{d}x'}{B_x} + \frac{B}{B_{\mathrm{in}}}V_{\parallel \mathrm{in}}, \tag{3}$$

where the subscript 'in' denotes the values at the inner midplane.

Accounting for diffusion and ∇B drift as the most important contributions to Eq. (1) we have

$$\left\langle\left\langle h_z m_i n(\widetilde{V}_y^{(\mathrm{dia})} + V_y^{(\mathrm{diff})})V_\parallel\right\rangle\right\rangle = \left\langle\left\langle h_z \eta\frac{\partial V_\parallel}{h_y \partial y}\right\rangle\right\rangle, \tag{4}$$

where $\widetilde{V}_y^{(\mathrm{dia})} = -\frac{T_i B}{e}\frac{\partial B^{-2}}{h_x \partial x}$ is the ∇B drift velocity and $V_y^{(\mathrm{diff})}$ is the radial diffusive velocity.

From Eqs. (3) and (4), the three components of momentum flux may be estimated as

$$\left\langle\left\langle h_z m_i n \widetilde{V}_y^{(\mathrm{dia})} V_\parallel\right\rangle\right\rangle \sim m_i \delta\frac{T_i}{e}\frac{I}{B_x};$$
$$\left\langle\left\langle h_z m_i n V_y^{(\mathrm{diff})} V_\parallel\right\rangle\right\rangle \sim \left\langle\left\langle h_z \eta\frac{\partial V_\parallel}{h_y \partial y}\right\rangle\right\rangle \sim R\eta\frac{\langle V_\parallel\rangle}{\lambda}, \tag{5}$$

where λ and δ are radial and poloidal scales of the source. Eqs. (4) and (5) yield:

$$\langle V_\parallel\rangle \sim \frac{T_i}{eRB_x}\delta\frac{m_i\lambda}{\eta}I \sim \frac{\widetilde{V}^{(\mathrm{dia})}B_{\mathrm{toroidal}}}{B_{\mathrm{poloidal}}}\frac{r}{\lambda}\frac{1}{\alpha}\left(\frac{\lambda^2 I}{nD}\frac{\delta}{r}\right), \tag{6}$$

where $\eta = \alpha n m_i D$. This estimate is reasonable when the source $I(x,y)$ which represents the gas puff, is localized. The expression in parenthesis in Eq. (6) is of the order of unity, if the source localized at the inner midplane and anomalous diffusion are the only factors determining plasma density.

The effect is very strong for the MAST parameters. The upper estimate is:

$$\frac{\widetilde{V}^{(\mathrm{dia})}B_{\mathrm{toroidal}}}{B_{\mathrm{poloidal}}} \approx 3\,\mathrm{km/s}, \quad \frac{r}{\lambda} \approx 20;$$
$$\langle V_\parallel\rangle \sim \frac{\widetilde{V}^{(\mathrm{dia})}B_{\mathrm{toroidal}}}{B_{\mathrm{poloidal}}}\frac{r}{\lambda} \sim 60\,\mathrm{km/s}. \tag{7}$$

In reality the major part of particle source is connected with recycling and is mainly situated at the outer part of torus. As a result the expression in parenthesis in Eq. (6) is less than unity and is proportional to the gas puff at the inner midplane. Therefore the distribution of parallel velocity is more gradual and the whole effect is an order of magnitude smaller. However, the parametric dependence, i.e. linear dependence on the ion temperature and inverse dependence on the plasma current are important predictions of the model.

4. Conclusions

It is demonstrated that counter-current toroidal torque can be generated by inboard gas puff by creating inboard/outboard parallel fluxes associated with the ionization source on the closed field lines. These fluxes are transported by the vertical ∇B ion drift providing counter-current acceleration. The model is qualitatively consistent with simulation results and might explain some MAST experiments.

Acknowledgments

This work was funded jointly by the United Kingdom Engineering and Physical Sciences Research Council and by EURATOM.

References

[1] A.R. Field et al., 30 EPS Conf. Controlled Fusion Plasma Physics, St. Petersburg, Russia, 2003, presentation 3.165.
[2] S.K. Erents et al., Plasma Phys. Control. Fusion 42 (2000) 905.
[3] N. Asakura et al., Phys. Rev. Lett. 84 (2000) 3093.
[4] J. Ghosh et al., Phys. Plasmas 11 (2004) 1033.
[5] V. Rozhansky et al., Nucl. Fusion 41 (2001) 387.
[6] T.D. Rognlien, D.D. Ryutov, N. Mattor, Czech. J. Phys. 48 (Suppl. S2) (1998) 201.
[7] A.V. Chankin et al., J. Nucl. Mater. 290–293 (2001) 518.
[8] T. Fullop, P. Helander, P.J. Catto, Phys. Rev. Lett. 89 (2002) 225003-1.
[9] H.A. Claassen, H. Gerhauser, A. Rogister, Phys. Plasmas 7 (2000) 3699.
[10] V. Rozhansky, M. Tendler, Phys. Plasmas 1 (1994) 2711.